Decay of metastable states with discrete dynamics

Peter Reimann,* Reinhard Müller,† and Peter Talkner
Paul Scherrer Institut, CH-5232 Villigen, Switzerland
(Received 20 December 1993)

We consider the escape from invariant sets of one-dimensional piecewise linear maps which are additively disturbed by weak Gaussian white noise. The escape rates from point attractors and from strange invariant sets in the vicinity of the crisis at fully developed chaos are analytically determined and compared with results from numerical simulations. Both situations are combined resulting in a model with a point attractor which has a strange invariant set as basin boundary. Numerically a nonexponential decay of the attractor is found that can be described by a Markovian three-state model with transition rates known from the previous analysis.

PACS number(s): 05.40.+j, 05.45.+b, 02.50.−r

I. INTRODUCTION

A basic property of many nonlinear dissipative dynamical systems is the coexistence of different basins of attraction. In a realistic description of most experimental situations one has to include the influence of random fluctuations on the system which may lead to transitions between these basins. Hence the decay of metastable states is of interest for various scientific areas and has been the subject of investigations for many decades [1,2].

In this paper we consider a one-dimensional dynamics in discrete time in the presence of Gaussian white noise. In comparison with a time-continuous system, a map may show a much richer behavior in one dimension such as, for example, periodic and strange invariant sets. At the same time, a nonlinear noisy map violates the principle of detailed balance even in one dimension [3] and, as a consequence, is much more difficult to handle [4–7] than the corresponding time-continuous system [8]. Both the rich dynamical behavior and the difficulties due to the absence of detailed balance are also found in continuous-time systems in more than one dimension [9].

Further, we restrict ourselves to piecewise linear maps which are disturbed by weak additive noise. The assumption of weak noise is crucial since at a too high noise level metastable states lose their identity and the rate concept becomes meaningless [2]. The other assumptions, namely, piecewise linearity of the map and additive noise coupling, are of a technical nature since, due to the lack of detailed balance, closed analytical expressions for rates are usually not available for more general processes in discrete time [10].

In Sec. II we consider the simplest case of escape from a basin of a point attractor. We adapt the basic idea of the reactive flux method [11] to processes in discrete time and in this way not only obtain the leading order behavior of the rate in the noise strength [10,12] but also all algebraic finite-noise corrections. In Sec. III we study hyperbolic maps in the chaotic regime near the crisis at fully developed chaos, considering in particular a strange attractor below the crisis, a marginally stable strange invariant set at the crisis, and a strange repeller beyond the crisis. In the latter case there is transient chaos governed by exponential decay even in the absence of noise [13]. The analytical results are compared with numerical simulations and the relation to previous investigations of similar systems is discussed.

In Sec. IV the situations considered in Secs. II and III are combined: Starting at a point attractor we investigate the decay of this metastable state in the case where the escape paths have to cross a strange invariant set. In particular this includes the case in which the basin boundary of the point attractor is a fractal set. We believe that this scenario is of rather broad interest due to the ubiquitous presence of both fractal structures [14] and noise [15] in nature. The escape over fractal basin boundaries has been observed in Josephson junctions [16], in a model for bistable chemical reactions [17], in the driven damped pendulum [18], and in a discrete-time version of Newton's second law including friction and fluctuating forces [19]. A similar two-dimensional situation has recently been investigated in [20]. We show in a numerical simulation that, in contrast to Secs. II and III, the decay can no longer be described by a single rate, i.e., it does not follow an exponential law if the time to reach the strange invariant set is comparable to the time to leave it again. We describe this behavior by means of a Markovian three-state model which, in combination with the analytical results of Secs. II and III, leads to excellent agreement with the numerical simulations. We close with a summary of our main results and a discussion of some interesting related problems for future investigations in Sec. V.

*Present address: Limburgs Universitair Centrum, B-3590 Diepenbeek, Belgium.
†Present address: Universität Leipzig, Institut für Theoretische Physik, Augustusplatz 10/11, D-04109 Leipzig, Germany.

II. DECAY OF A POINT ATTRACTOR

In this section we consider a piecewise linear map with a point attractor and an unstable fixed point disturbed by weak Gaussian white noise. While in [5,10,12] the rate of escape from the point attractor over the unstable fixed point was determined by means of Kramers's flux-over-population method [1], here we treat a nonstationary situation in which an initial ensemble of particles is distributed near the stable fixed point and eventually decays away. This approach not only gives the weak-noise limit of the decay rate but also all algebraic finite-noise corrections and turns out to agree very well with numerical simulations.

We consider a one-dimensional dynamical system in discrete time n additively coupled to independent, identically distributed Gaussian noise ξ_n:

$$x_{n+1}=f(x_n)+\xi_n, \quad P(\xi_n)=\frac{1}{\sqrt{\pi\epsilon}}e^{-\xi_n^2/\epsilon} . \tag{2.1}$$

The noise strength ϵ is assumed to be small and the map $f(x)$ to be piecewise linear with simple stable and unstable fixed points at $x_s>0$ and $x_u=0$, respectively,

$$\begin{aligned} f(x)&=x_s+s(x-x_s) \quad \text{for } x\geq x_m , \\ f(x)&=ux \quad \text{for } x\leq x_m , \end{aligned} \tag{2.2}$$

where x_m is the matching point of the two linear pieces

$$x_m=\frac{1-s}{u-s}x_s . \tag{2.3}$$

The stability properties of the fixed points x_s and x_u require $u>1$ and $-1<s<1$. For the sake of convenience we further restrict ourselves to non-negative values of s. Then, $\mathbb{R}_+$ is the basin of attraction of the stable fixed point x_s whereas $\mathbb{R}_-$ may be considered as the basin of an attractor at $-\infty$.

From the discrete-time Langevin equation (2.1) one finds for the transition probability $P(x|y)$ to get from y to x in one time step that

$$\begin{aligned} P(x|y)&=\int_{-\infty}^{\infty} d\xi\, \delta(x-f(y)-\xi)P(\xi) \\ &=\frac{1}{\sqrt{\pi\epsilon}}e^{-[x-f(y)]^2/\epsilon} . \end{aligned} \tag{2.4}$$

The time evolution of the probability densities $W_n(x)$ to find the system in state x at time n is governed by the master equation

$$W_{n+1}(x)=\int_{-\infty}^{\infty} dy\, P(x|y)W_n(y) . \tag{2.5}$$

The time-dependent decay rate $k(n)$ is given by the relative decrease of the population within the basin $\mathbb{R}_+$ of the point attractor x_s:

$$k(n)=\frac{\int_0^{\infty} dx\, W_{n-1}(x)-\int_0^{\infty} dx\, W_n(x)}{\int_0^{\infty} dx\, W_{n-1}(x)} . \tag{2.6}$$

Since the total population is conserved the decrease of population of $\mathbb{R}_+$ equals the increase of population of $\mathbb{R}_-$. Therefore the rate can equivalently be expressed as

$$k(n)=\frac{\int_{-\infty}^{0} dx\, W_n(x)-\int_{-\infty}^{0} dx\, W_{n-1}(x)}{\int_0^{\infty} dx\, W_{n-1}(x)} . \tag{2.7}$$

In the limit of small noise, in which a rate description is meaningful, the rate itself is very small, i.e., the number of particles leaving $\mathbb{R}_+$ in one time step is always much smaller than the actual population of $\mathbb{R}_+$. Therefore the numerator of (2.6) is given by the difference of two large numbers. On the other hand, when the initial distribution is concentrated about the attractor x_s the population of $\mathbb{R}_-$ remains much smaller than that of $\mathbb{R}_+$ for quite a large number of iterations. Being the difference of the smaller populations of $\mathbb{R}_-$ the numerator of (2.7) represents a more reliable expression of the flux, particularly when the time dependence of the density is only approximately known.

At sufficiently small noise a clear-cut separation of two different time scales can be observed: A very slow one is determined by the inverse $1/k$ of the asymptotic rate $k=\lim_{n\to\infty}k(n)$ and a fast one describes the rate of convergence towards this limit. These time scales are clearly related to the fast relaxational motion inside the basin $\mathbb{R}_+$, which establishes there a quasi-invariant density $W(x)$, and to the infrequent escape from $\mathbb{R}_+$, which leads to a slow exponential decay of the quasi-invariant state [2,11].

In order to determine the asymptotic rate k we start with a Gaussian initial distribution $W_0(x)$:

$$W_0(x)=\left[\frac{1-s^2}{\pi\epsilon}\right]^{1/2} e^{-(1-s^2)[x-x_s]^2/\epsilon} , \tag{2.8}$$

which according to the master equation (2.5) goes in one time step over into $W_1(x)$:

$$\begin{aligned} W_1(x)=&\int_{-\infty}^{x_m}\frac{dy}{\sqrt{\pi\epsilon}}\left[\frac{1-s^2}{\pi\epsilon}\right]^{1/2} e^{-\{(1-s^2)[y-x_s]^2+[x-uy]^2\}/\epsilon} \\ &+\int_{x_m}^{\infty}\frac{dy}{\sqrt{\pi\epsilon}}\left[\frac{1-s^2}{\pi\epsilon}\right]^{1/2} e^{-\{(1-s^2)[y-x_s]^2+[x-x_s-s(y-x_s)]^2\}/\epsilon} . \end{aligned} \tag{2.9}$$

Both integrals on the right hand side (rhs) of (2.9) can be exactly expressed as products of a Gaussian and a complementary error function. Unfortunately, the further time evolution of the density cannot be followed exactly. Therefore we give an approximate form of $W_1(x)$ whose time evolution can be determined for a sufficient number of time steps with a relative error being exponentially small in the noise strength ϵ. In the first integral of (2.9) the error function assumes the constant value 2 besides exponentially small deviations provided $x<x_1$ with

$$x_1=\frac{1+(u-s)(u-1)}{u}x_m \ . \tag{2.10}$$

Consequently, for $x<x_1$ the first integral is well approximated by a Gaussian function which reads as follows:

$$\int_{-\infty}^{x_m}\frac{dy}{\sqrt{\pi\epsilon}}\left[\frac{1-s^2}{\pi\epsilon}\right]^{1/2}e^{-\{(1-s^2)[y-x_s]^2+[x-uy]^2\}/\epsilon}$$

$$=\left[\frac{a_1}{\pi\epsilon}\right]^{1/2}e^{-a_1[x-ux_s]^2/\epsilon}, \tag{2.11}$$

where $a_1=(1-s^2)/[1-s^2+u^2]$. For $x\geq x_1$ the error function rapidly decreases, and consequently the right hand side of Eq. (2.11) represents an upper bound to the first integral.

The second integral of Eq. (2.9) can be approximated in an analogous way. As we restrict ourselves to nonnegative s the integral coincides with $W_0(x)$ for all $x>x_2$ besides an exponentially small relative error:

$$\int_{x_m}^{\infty}\frac{dy}{\sqrt{\pi\epsilon}}\left[\frac{1-s^2}{\pi\epsilon}\right]^{1/2}$$

$$\times e^{-\{(1-s^2)[y-x_s]^2+[x-x_s-s(y-x_s)]^2\}/\epsilon}=W_0(x), \tag{2.12}$$

where

$$x=\frac{1+s-u}{s}x_m \ . \tag{2.13}$$

For x values smaller than x_2 the multiplying complementary error function decreases and the right hand side of (2.12) represents an upper bound to the second integral of Eq. (2.9). With $s\geq 0$ one finds $x_2<x_1$, i.e., the ranges of validity of the Gaussian approximations (2.11) and (2.12) overlap. The Gaussians intersect in the point x_0:

$$x_0=\frac{(1-s^2+u^2)^{1/2}-u}{(1-s^2+u^2)^{1/2}-1}x_s \ , \tag{2.14}$$

which falls into the interval $[x_2,x_1]$ for $s\geq 0$. For $x<x_0$ the first integral of Eq. (2.9) dominates and for $x>x_0$ the second one. The matching point x_m is always larger than x_0. Since sufficiently far away from x_0 the Gaussian approximations (2.11) and (2.12) differ from each other by a factor which is exponentially large in ϵ, the first term in (2.9) may be neglected for $x>x_m$ and the second one may even be replaced by the Gaussian contribution (2.12) for $x\leq x_2$. In this way we find the following approximation for $W_1(x)$ which deviates only by an exponentially small function from its true form:

$$W_1(x)=\Theta(x_m-x)\left[\frac{a_1}{\pi\epsilon}\right]^{1/2}e^{-a_1[x-ux_s]^2/\epsilon}+W_0(x) \ , \tag{2.15}$$

where $\Theta(x)$ equals unity for positive x and vanishes otherwise. The further time evolution can now be obtained by means of the same arguments leading to the following recursive relation:

$$W_n(x)=\Theta(x_m-x)\left[\frac{a_n}{\pi\epsilon}\right]^{1/2}e^{-a_n[x-u^nx_s]^2/\epsilon}+W_{n-1}(x) \ , \tag{2.16}$$

where $a_n=(u^2-1)(1-s^2)/[u^{2n}(u^2-s^2)-(1-s^2)]$. A different derivation of the density $W_n(x)$ in the limit $n\to\infty$ may be found in Ref. [10].

With (2.16) the rate $k(n)$ readily follows from Eq. (2.7) yielding besides exponentially small corrections in ϵ

$$k(n)=\tfrac{1}{2}\mathrm{erfc}\left[x_s\left[\frac{(u^2-1)(1-s^2)}{[u^2-s^2-(1-s^2)u^{-2n}]\epsilon}\right]^{1/2}\right], \tag{2.17}$$

where $\mathrm{erfc}(x):=2\pi^{-1/2}\int_x^{\infty}\exp\{-y^2\}dy$ is the complementary error function. Indeed, this result shows the expected convergence for large n and yields for the asymptotic rate $k=\lim_{n\to\infty}k(n)$

$$k=\tfrac{1}{2}\mathrm{erfc}(\sqrt{\Delta\phi/\epsilon}) \ , \tag{2.18}$$

where $\Delta\phi=x_s^2(u^2-1)(1-s^2)/[u^2-s^2]$ is the difference of the so-called generalized potential at the fixed points x_s and $x=0$ [3,10]. In an equilibrium system the ratio $\Delta\phi/\epsilon$ corresponds to the barrier height divided by the thermal energy. Since this quantity is larger than unity, one may use the asymptotic series expansion of the complementary error function:

$$\mathrm{erfc}(x)=\frac{e^{-x^2}}{\sqrt{\pi}x}\left[1-\frac{1}{2}\frac{1}{x^2}+\frac{1}{2}\frac{3}{2}\frac{1}{x^4}-\frac{1}{2}\frac{3}{2}\frac{5}{2}\frac{1}{x^6}+\cdots\right]. \tag{2.19}$$

This yields for the rate k

$$k=\left[\frac{\epsilon}{4\pi\Delta\phi}\right]^{1/2}e^{-\Delta\phi/\epsilon}\left[1-\frac{1}{2}\frac{\epsilon}{\Delta\phi}+\frac{3}{4}\left[\frac{\epsilon}{\Delta\phi}\right]^2-\cdots\right]. \tag{2.20}$$

The factor in front of the square brackets on the right hand side represents the leading part of the rate as it was obtained in Ref. [10]. As for the rate of a one-dimensional Smoluchowski process in continuous time the leading part is exponentially small in the barrier height measured in units of the noise strength [1,2], but in contradistinction to a Smoluchowski rate the preexponential factor depends on the noise strength. In the square brackets a series in powers of the ratio of the noise strength and the barrier height describes the algebraic finite ϵ corrections to the leading order behavior. Without going into further details we note that the expression (2.18) remains valid for negative values of s provided $s>-u/[u+1]$. For smaller values of s Eq. (2.18) is no longer correct as may be seen from Table III below.

The particular form of the time-dependent rate (2.17) only applies for the initial density (2.8). Although in general different initial densities lead to different time-dependent rates, we may nevertheless expect that not

only the asymptotic rate k but also the time scale n_0 on which the convergence of $k(n)$ takes place are independent of the initial density provided it is concentrated around the stable fixed point x_s. From Eq. (2.17) one finds for n_0

$$n_0=\ln\left[\frac{\Delta\phi}{\epsilon}\frac{1-s^2}{u^2-s^2}\right]\Big/\ln u\ . \tag{2.21}$$

For small noise this time scale is always much shorter than the inverse rate $1/k$ confirming our assumption about a clear-cut separation of time scales, see the discussion below Eq. (2.7). Finally, we note that for a superstable fixed point with $s=0$ any initial distribution that vanishes for $x<x_m$ is mapped in one time step on the density $W_0(x)$ given by (2.8) and consequently leads to the time-dependent rate (2.17).

For a numerical check of our results we proceed as follows: We numerically simulate trajectories of the Langevin equation (2.1) with initial condition $x_0=x_s$ until a trajectory passes a threshold $x_{\rm th}$, which lies well beyond the unstable point $x_u=0$, or until a properly chosen maximal time T has elapsed. The threshold $x_{\rm th}$ is chosen such that the probability of return into the initial domain of attraction becomes negligible. From N realizations we estimate the probability $P(n)$ that the threshold $x_{\rm th}$ has been passed for the first time after n time steps, $n\le T$. Typical values in the simulations leading to Figs. 1 and 3 and Table IV are $10^2\le T\le 10^4$ and $N=5\times10^5$.

In order to find a reasonable value for $x_{\rm th}$ we note that the probability $p(x_{\rm th})$ to leave the interval $[-\infty,x_{\rm th}]$ is approximately given by the probability to leave it in one step: Since for sufficiently large values of $x_{\rm th}$ the probability flows almost deterministically, a flow out of the interval in two or more steps can safely be neglected. Hence one finds

$$p(x_{\rm th})\simeq\tfrac{1}{2}\mathrm{erfc}\left[-\frac{[u-1]x_{\rm th}}{\sqrt{\epsilon}}\right]\simeq\frac{\sqrt{\epsilon}e^{-[u-1]^2x_{\rm th}^2/\epsilon}}{2\sqrt{\pi}[u-1]|x_{\rm th}|}\ , \tag{2.22}$$

where we made use of (2.19) (e.g., for $[u-1]^2x_{\rm th}^2/\epsilon=5$ and 10, $p(x_{\rm th})$ is about 10^{-3} and 10^{-5}, respectively). In the simulations we choose $x_{\rm th}$ such that $p(x_{\rm th})<10^{-4}$.

The escape probability $P(n)$ coincides with the flux out of the interval $[x_{\rm th},\infty]$. It reads in terms of the densities at times $n-1$ and n, which follow from an appropriate initial density by means of the master equation (2.5):

$$P(n)=\int_{x_{\rm th}}^{\infty}dx\,[W_{n-1}(x)-W_n(x)]\ . \tag{2.23}$$

In analogy to Eq. (2.6) the flux is given by a time-dependent rate $\tilde{k}(n)$ and the population of the interval $[x_{\rm th},\infty]$ at time $n-1$:

$$\int_{x_{\rm th}}^{\infty}dx\,[W_{n-1}(x)-W_n(x)]=\tilde{k}(n)\int_{x_{\rm th}}^{\infty}dx\ W_{n-1}(x)\ . \tag{2.24}$$

With the initial condition $\int_{x_{\rm th}}^{\infty}dx\ W_0(x)=1$ the rates $\tilde{k}(n)$ can be expressed in terms of the escape probabilities $P(i)$, $i\le n$:

$$\tilde{k}(n)=\frac{P(n)}{1-\sum_{i=1}^{n-1}P(i)}\ . \tag{2.25}$$

We note that this relation is useful for the determination of the time-dependent rate and its asymptotic limit from numerical simulations. On the other hand, Eqs. (2.23) and (2.24) can be solved for the escape probabilities $P(n)$ as a function of the rates $\tilde{k}(i)$, $i\le n$:

$$P(n)=[1-\tilde{k}(1)][1-\tilde{k}(2)]\cdots[1-\tilde{k}(n-1)]\tilde{k}(n)\ . \tag{2.26}$$

TABLE I. The time-dependent rates $\tilde{k}(n)$ defined in Eq. (2.24) for the noisy map (2.1) and (2.2) with $x_s=1$, $s=0$, $u=2$, $\epsilon=0.1$, and initial distribution (2.8). Columns (1) and (3): results from numerical integration of the master equation according to (2.28) with thresholds $x_{\rm th}=-0.5$ and -1, respectively (the numerical error is below 0.1%). Columns (2) and (4): theoretical results (2.27) for the same thresholds $x_{\rm th}=-0.5$ and -1, respectively. In agreement with the theory, for large n the rates approach an asymptotic value independent of the threshold. Note that for $x_{\rm th}=-1$ the rates are approximately shifted by one time step in comparison with $x_{\rm th}=-0.5$.

n	(1)	(2)	(3)	(4)
1	2.864×10^{-7}	2.867×10^{-7}	9.867×10^{-10}	9.866×10^{-10}
2	5.623×10^{-6}	5.627×10^{-6}	5.318×10^{-7}	5.318×10^{-7}
3	1.860×10^{-6}	1.869×10^{-6}	6.321×10^{-6}	6.338×10^{-6}
4	3.185×10^{-5}	3.222×10^{-5}	1.905×10^{-5}	1.919×10^{-5}
5	4.115×10^{-5}	4.187×10^{-5}	3.204×10^{-5}	3.242×10^{-5}
6	4.662×10^{-5}	4.743×10^{-5}	4.121×10^{-5}	4.184×10^{-5}
7	4.957×10^{-5}	5.051×10^{-5}	4.663×10^{-5}	4.745×10^{-5}
8	5.110×10^{-5}	5.211×10^{-5}	4.957×10^{-5}	5.051×10^{-5}
9	5.188×10^{-5}	5.292×10^{-5}	5.110×10^{-5}	5.211×10^{-5}
10	5.228×10^{-5}	5.334×10^{-5}	5.188×10^{-5}	5.293×10^{-5}
15	5.266×10^{-5}	5.374×10^{-5}	5.265×10^{-5}	5.373×10^{-5}
20	5.267×10^{-5}	5.376×10^{-5}	5.267×10^{-5}	5.376×10^{-5}

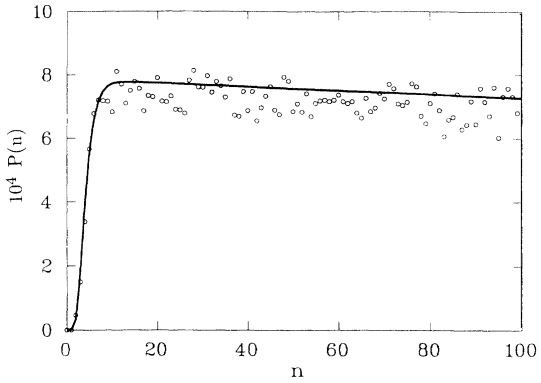

FIG. 1. The probability $P(n)$ to leave the domain $[x_{\rm th},\infty]$ at time n for the first time $0\le n\le T=100$ for the noisy map (2.1) and (2.2) with initial condition $x_{-1}=x_s$. The values of the parameters are $u=2$, $s=0$, $x_s=1$, $x_{\rm th}=-1$, and $\epsilon=0.15$. The dots represent the numerical results from $N=5\times10^5$ realizations of the Langevin equation (2.1) and the solid line is the theoretical prediction (2.26) and (2.27).

Starting from the initial condition $W_0(x)$ given in Eq. (2.8) one can determine the rate $\tilde{k}(n)$ in the same way as $k(n)$ in Eq. (2.17) with the following result:

$$\tilde{k}(n)=\tfrac{1}{2}\mathrm{erfc}\left[\left[\frac{(u^2-1)(1-s^2)}{[u^2-s^2-(1-s^2)u^{-2n}]\epsilon}\right]^{1/2}\times\left[x_s-\frac{x_{\rm th}}{u^n}\right]\right], \tag{2.27}$$

which is displayed for a particular choice of parameters in Table I. Note that the rate $\tilde{k}(n)$ approaches the same large-n limit (2.18) as $k(n)$ in Eq. (2.17). Inserted into Eq. (2.26) the time-dependent rates determine the theoretical escape probabilities which are compared to the corresponding results from a numerical simulation in Fig. 1.

If ϵ is small or if a high accuracy of the rate $\tilde{k}(n)$ is required, the simulation of the Langevin equation (2.1) becomes extremely expensive. Alternatively, one may numerically iterate the master equation with an absorbing region for $x<x_{\rm th}$. Then the rate $\tilde{k}(n)$ is given by the ratio of the probability being absorbed at time n and the population of the interval $[x_{\rm th},\infty]$ at time $n-1$:

$$\tilde{k}(n)=\frac{\int_{-\infty}^{x_{\rm th}}dx\int_{x_{\rm th}}^{\infty}dy\,P(x|y)W_{n-1}(y)}{\int_{x_{\rm th}}^{\infty}dx\,W_{n-1}(x)}. \tag{2.28}$$

It turns out that this procedure needs less numerical effort for small noise ϵ than simulations of the Langevin equation. Starting with the initial distribution (2.8) [strictly speaking with an additional factor $\Theta(x-x_{\rm th})$ on the rhs] it is possible to compare the numerical results from (2.28) with the theoretical prediction (2.27) also for $s\neq0$. Table I shows the convergence of $\tilde{k}(n)$ for different values of the threshold $x_{\rm th}$. Tables II and III give additional numerical evidence that the asymptotic values of the rates $k(n)$ and $\tilde{k}(n)$ are independent of $x_{\rm th}$ and agree with each other. In summary, the numerical results of Fig. 1 and Tables I–III agree very well with our analytical time-dependent and asymptotic rates. For sufficiently small noise the deviations indeed are exponentially small in the noise strength in accordance with the prediction.

TABLE II. The asymptotic decay rate $k=\lim_{n\to\infty}k(n)=\lim_{n\to\infty}\tilde{k}(n)$ for noisy maps (2.1) and (2.2) with $x_s=1$ and different values of ϵ, u, and s. The first number is the numerical rate $k_{\rm num}$ from iterated probability densities evaluated according to (2.28). The number below is the relative difference in percent $100[k-k_{\rm num}]/k_{\rm num}$ to the theoretical results k in (2.18). For sufficiently small values of the noise strength ϵ the agreement between numerical simulations and analytical results is essentially limited by the finite numerical accuracy. The agreement is particularly good for small $|s|$ and large u. The number in parentheses gives the same relative difference in percent but for the leading part of the theoretical result on the rhs of (2.20) without the algebraic corrections in parentheses. As predicted by (2.20), this relative difference becomes proportional to the noise strength ϵ for sufficiently small ϵ.

ϵ	$s=0,u=2$	$s=0,u=5$	$s=0.5,u=2$	$s=0.5,u=5$	$s=-0.5,u=2$	$s=-0.5,u=5$
0.4	2.093×10^{-2}	1.376×10^{-2}	2.216×10^{-2}	2.021×10^{-2}	3.202×10^{-2}	2.584×10^{-2}
	26 (51)	3.4 (20)	88 (132)	40 (68)	30 (61)	9.5 (32)
0.2	2.789×10^{-3}	9.668×10^{-4}	4.605×10^{-3}	2.930×10^{-3}	5.760×10^{-3}	3.276×10^{-3}
	11 (23)	0.6 (10)	55 (76)	20 (33)	24 (41)	6.9 (19)
0.1	5.268×10^{-5}	5.885×10^{-6}	2.093×10^{-4}	6.461×10^{-5}	2.261×10^{-4}	6.681×10^{-5}
	2.0 (8.1)	0.02 (4.8)	27 (36)	5.9 (12)	18 (26)	2.4 (8.7)
0.05	2.158×10^{-8}	2.882×10^{-10}	4.817×10^{-7}	3.424×10^{-8}	4.313×10^{-7}	3.443×10^{-8}
	0.1 (3.3)	−0.001 (2.5)	9.8 (14)	0.9 (4.1)	12 (16)	0.3 (3.5)
0.025	4.743×10^{-15}	9.459×10^{-19}	2.092×10^{-12}	1.195×10^{-14}	2.064×10^{-12}	1.195×10^{-14}
	−0.005 (1.6)	−0.001 (1.3)	1.9 (3.9)	0.03 (1.7)	3.3 (5.3)	0.004 (1.7)
0.012 5	3.163×10^{-28}	1.416×10^{-35}	5.739×10^{-23}	1.978×10^{-27}	5.688×10^{-23}	1.978×10^{-27}
	−0.007 (0.8)	−0.001 (0.06)	0.09 (1.1)	−0.005 (0.8)	1.0 (2.0)	−0.002 (0.8)
0.006 25	1.967×10^{-54}	4.448×10^{-69}	5.818×10^{-44}	7.578×10^{-53}	5.815×10^{-44}	7.578×10^{-53}
	−0.006 (0.4)	0.002 (0.3)	−0.005 (0.5)	−0.002 (0.4)	0.05 (0.6)	−0.002 (0.4)
0.003 125	1.068×10^{-106}	6.176×10^{-136}	8.377×10^{-86}	1.563×10^{-103}	8.377×10^{-86}	1.563×10^{-103}
	−0.008 (0.2)	0.005 (0.2)	0.006 (0.03)	0.004 (0.2)	−0.006 (0.3)	0.004 (0.2)

TABLE III. The relative difference in percent $100[k-k_{\text{num}}]/k_{\text{num}}$ of the theoretical result k in (2.18) and the numerical rates k_{num} from iterated probability densities in (2.28) for the noisy map (2.1) and (2.2) with $x_s=1$ and different values of s and u for three fixed theoretical rates $k=10^{-3}$, 10^{-6}, and 10^{-10} (from above). As in Table II, the best agreement between theory and numerics is achieved for small $|s|$ and large u. Theoretically, the deviations are predicted to be given in leading order by a sum of terms of the form $\exp\{-c/\epsilon\}$, where c is a non-negative number depending on x_s, u, and s but not on ϵ. It follows that at least one of the c's approach zero for $u\to 1$, $s\to 1$, or $s\to -u/[u+1]$. In agreement with the theoretical prediction mentioned in the main text, the rate formula (2.18) fails for $s<-u/[u+1]$ and the relative differences explode.

	$s=0.9$	$s=0.7$	$s=0.5$	$s=0.3$	$s=0.1$	$s=0$	$s=-0.1$	$s=-0.3$	$s=-0.5$	$s=-0.7$	$s=-0.9$	$u/[u+1]$
	448	205	132	95	71	62	56	50	63	156	6×10^3	
$u=1.2$	272	113	63	37	22	18	15	15	40	265	6×10^5	$0.5\overline{4}$
	187	69	34	17	7.6	5.6	4.3	6.6	38	599	2×10^8	
	275	109	63	38	24	19	16	15	32	146	2×10^5	
$u=1.5$	156	54	25	11	4.8	3.0	2.1	3.9	26	282	2×10^6	0.6
	103	28	10	3.4	0.8	0.4	0.2	1.4	21	507	1×10^9	
	210	71	35	18	9.2	6.6	5.1	6.0	20	113	1×10^4	
$u=2$	108	29	11	3.7	1.0	0.5	0.3	1.2	12	159	3×10^5	$0.\overline{6}$
	63	13	3.2	0.6	0.06	0.009	0.007	0.2	6.6	188	3×10^7	
	168	48	20	8.7	3.4	2.1	1.5	2.3	11	66	2×10^3	
$u=3$	77	16	4.5	1.0	0.2	0.05	0.03	0.2	3.6	53	1×10^4	0.75
	40	5.4	0.8	0.07	0.001	−0.002	−0.002	0.008	0.8	41	1×10^5	
	144	36	13	4.6	1.3	0.66	0.41	0.89	5.0	31	6×10^2	
$u=5$	59	10	2.0	0.3	0.03	0.005	0.003	0.04	0.8	14	9×10^2	$0.8\overline{3}$
	29	2.4	0.2	0.009	0.001	−0.001	−0.001	−0.001	0.06	6.3	2×10^3	

III. DECAY IN THE VICINITY OF A CRISIS

In this section we study noisy piecewise linear maps near the crisis at fully developed chaos. It is well known that above the crisis both with and without noise the system rapidly approaches a pseudostationary state obeying an exponential decay law [13,21]. The analytical and numerical investigations of this section confirm the exponential decay for noisy maps at and below the crisis. In the main part we confine ourselves to a particularly simple map consisting of two linear pieces. Results for more general cases are stated at the end.

We consider the Langevin equation (2.1) for the hyperbolic map $f(x)$ given by

$$f(x)=\begin{cases} ux & \text{for } x\geq -L/2 \\ u(x+L)-L & \text{for } x<-L/2\ , \end{cases} \tag{3.1}$$

where the slope u is assumed to be close to 2,

$$|u-2|\ll 1\ . \tag{3.2}$$

The map $f(x)$ has two unstable fixed points at $x=0$ and $-L$ and is symmetric about $x=-L/2$. For $u<2$ there is a strange attractor with basin $I=[-L,0]$. At $u=2$ one has fully developed chaos at a crisis, i.e., the unstable fixed points collide with the marginally stable strange attractor [22]. For $u>2$ the map $f(x)$ has a strange repeller on the interval I [13].

Independent of the actual value of u, the probability density $W_n(x)$ obeys the master equation (2.5). The time-dependent decay rate $k(n)$ is given by an expression analogous to Eq. (2.6) in which the integrals are extended over I rather than $\mathbb{R}_+$. In an expression for $k(n)$ corresponding to Eq. (2.7) the integral over $\mathbb{R}_-$ is replaced by one over the complement of I. When one starts with an initial distribution $W_0(x)$ that is symmetric about $x=-L/2$, $W_n(x)$ retains the same symmetry for all $n>0$, and the rate (2.7) takes the form

$$k(n)=\frac{\int_0^\infty dx\ W_n(x)-\int_0^\infty dx\ W_{n-1}(x)}{\int_{-L/2}^0 dx\ W_{n-1}(x)}\ . \tag{3.3}$$

Note that the rate $k(n)$ includes both the escapes to $+\infty$ and $-\infty$ which for symmetry reasons occur with equal probabilities.

For $u>2$ there is a decay even without noise. For large n the rate $k(n)$ converges towards an asymptotic value k and in the same limit the density $W_n(x)$ approaches a constant value times e^{-kn} on the strange repeller I [13]. Hence the asymptotic decay rate k is simply given by the fraction of the interval I that is mapped outside I under $f(x)$, i.e.,

$$k=\frac{u-2}{u}\ . \tag{3.4}$$

In the absence of noise the strange repeller in I can be left only through a small vicinity of $x=-L/2$. A later return into I is impossible. In the presence of noise, escapes are possible both for $u>2$ and $u\leq 2$. As in the deterministic case, a typical noisy escape path also visits the neighborhood of $x=-L/2$. From there it continues to the neighborhood of either $x=0$ and $-L$. Each of these unstable points may be recrossed several times until the path either definitely leaves the interval I or is again captured in I. Escape paths that do not visit the neighborhoods of $x=-L/2$ and $x=-L$ or 0 are extremely infrequent so that they can be neglected. However, the influence of the dynamics in the vicinity of the unstable fixed points on the escape rate is important and we take it

fully into account. In previous works it has often been neglected [23–25] or has been dealt with only approximately [26,27].

Before discussing the general case we briefly mention two limiting cases that should be contained in the full result: if $u>2$ and ϵ is sufficiently small, direct escapes from the vicinity of $x=-L/2$ without backscattering near either $x=0$ or $-L$ dominate; under these conditions we expect to recover the deterministic rate expression (3.4). On the other hand, for $u<2$ and ϵ sufficiently small, direct escapes from $x=-L/2$ are rare and the rate is dominated by the exits over the unstable points at $x=0$ and $-L$. In this case, the rate can be determined along the line of reasoning outlined in Sec. II. It results in [10]

$$k=\frac{\sqrt{\epsilon}}{2\sqrt{\pi}uLv^2}\left[\frac{u^2}{u^2-1}\right]^{3/2}e^{-(u^2-1)v^2/u^2}, \tag{3.5}$$

where

$$v=\frac{L}{\sqrt{\epsilon}}\frac{u-2}{2}. \tag{3.6}$$

The assumptions in the derivation of this result are $1\gg 2-u\gg\sqrt{\epsilon}/L$, i.e., $v\ll -1$.

Now we come back to the general case and construct a time-dependent symmetric solution of the master equation (2.5) for the map (3.1) from which the rate can be determined in an analogous way as in Sec. II. For this purpose we differentiate the master equation with respect to x and obtain

$$W'_{n+1}(x)=\int_{-\infty}^{-L/2}\frac{dy}{\sqrt{\pi\epsilon}}W_n(y)\frac{\partial}{\partial x}e^{-[x+L-u(y+L)]^2/\epsilon}+\int_{-L/2}^{\infty}\frac{dy}{\sqrt{\pi\epsilon}}W_n(y)\frac{\partial}{\partial x}e^{-[x-uy]^2/\epsilon}. \tag{3.7}$$

The derivatives with respect to x on the right hand side can be expressed in terms of the derivative with respect to y: $\partial/\partial x\to -u^{-1}\partial/\partial y$. A subsequent partial integration then yields

$$W'_{n+1}(x)=-\int_{-L/2}^{\infty}\frac{dy}{u\sqrt{\pi\epsilon}}W'_n(y)e^{-[x+L+uy]^2/\epsilon}+\int_{-L/2}^{\infty}\frac{dy}{u\sqrt{\pi\epsilon}}W'_n(y)e^{-[x-uy]^2/\epsilon}+\frac{W_n(-L/2)}{u\sqrt{\pi\epsilon}}\{e^{-[x+Lu/2]^2/\epsilon}-e^{-[x-L(u-2)/2]^2/\epsilon}\}, \tag{3.8}$$

where we used the symmetry $W_n(-L/2+y)=W_n(-L/2-y)$ in the first integral on the rhs.

Next we show that the function

$$W'_n(x)=-\frac{W}{u\sqrt{\pi\epsilon}}\sum_{i=0}^{n}\left[\frac{u^2-1}{u^2-u^{-2i}}\right]^{1/2}\frac{1}{u^{2i}}\times\exp\left\{-\frac{u^2-1}{u^2-u^{-2i}}\times\frac{\left[x-u^iL\frac{u-2}{2}\right]^2}{u^{2i}\epsilon}\right\} \tag{3.9}$$

solves (3.8) in good approximation if $x\geq -L/2$, $n\gg 1$, and the noise strength is sufficiently small,

$$\sqrt{\epsilon}\ll L. \tag{3.10}$$

Here W is a yet undetermined normalization constant. As a consequence of the conditions (3.2) and (3.10), $W'_n(x)$ has a very narrow peak near $x=0$. Hence the lower boundary $-L/2$ of the second integral in (3.8) can be replaced by $-\infty$ for all $x\in[-L/2,\infty]$, and the first integral can be neglected. Similarly, the first term in the curly brackets is negligibly small compared to the second one. The integration of (3.9) from x to $+\infty$ gives

$$W_n(x)=\frac{W}{2u}\sum_{i=0}^{n}u^{-i}\operatorname{erfc}\left\{\left[\frac{u^2-1}{u^2-u^{-2i}}\right]^{1/2}\times\left[\frac{xu^{-i}}{\sqrt{\epsilon}}-v\right]\right\}, \tag{3.11}$$

where v is defined in Eq. (3.6) and $W_n(\infty)$ has been set equal to zero in order to obtain a normalizable density. For $x=-L/2$ the complementary error functions that notably contribute to the sum in Eq. (3.11) can be approximated by $\operatorname{erfc}(-\infty)=2$. Since u differs from 2 only by a negligible amount, one finds $W_n(-L/2)=W$ for $n\gg 1$. Finally, it remains to show that $W'_n(x)$ as given by (3.9) fulfills the following integral equation:

$$W'_{n+1}(x)=\int_{-\infty}^{\infty}\frac{dy}{u\sqrt{\pi\epsilon}}W'_n(y)e^{-[x-uy]^2/\epsilon}-\frac{W}{u\sqrt{\pi\epsilon}}e^{-[x-L(u-2)/2]^2/\epsilon}. \tag{3.12}$$

This can be easily verified by inspection.

In summary, for $x\geq -L/2$, $n\gg 1$, $\sqrt{\epsilon}\ll L$, and $|u-2|\ll 1$, Eq. (3.11) represents an approximate solution of the differentiated master equation (3.8). With the symmetry about $x=-L/2$ the density $W_n(x)$ is determined for all values of x.

In the limiting case $v\ll -1$, near the unstable fixed points, the density $W_n(x)$ in Eq. (3.11) has the same structure as the corresponding one for the escape over a single fixed point; see Eq. (2.16). This is in agreement with the findings of Refs. [3,10]. In the opposite limit $v\gg 1$, $W_n(x)$ approaches a constant value on the interval $I=[-L,0]$ and in particular on the strange repeller as one may expect from the noiseless case as discussed in

the paragraph above Eq. (3.4). However, it does not properly decrease in time with the fact e^{-kn}. But this error is completely negligible on the relevant time scale on which the time-dependent rate $k(n)$ converges to its asymptotic value; see Eqs. (3.13) and (3.15). A similar method for the determination of invariant densities of higher-dimensional noisy maps has recently been employed by García-Pelayo and Schieve [28], however, with much less explicit results than those presented here.

Next we evaluate the time-dependent rate (3.3) following from the density (3.11). The integral in the denominator of the rate (3.3) is easily performed. As the derivative $W_n'(x)$ has a dominant peak near $x=0$, on the interval $[-L/2,0]$ the density $W_n(x)$ almost equals the constant value W except within a small vicinity of $x=0$. Hence the denominator of the rate can be approximated by $WL/2$. In the numerator of the rate all but one term stemming from the sum in Eq. (3.11) cancel each other leading to the following expression for the rate valid for $n \gg 1$:

$$k(n)=\frac{\int_0^\infty dx\, u^{-n}\operatorname{erfc}\left[\left[\frac{u^2-1}{u^2-u^{-2n}}\right]^{1/2}\left[\frac{xu^{-n}}{\sqrt{\epsilon}}-v\right]\right]}{uL} . \tag{3.13}$$

By means of the identity

$$\int_0^\infty dx\, \operatorname{erfc}(ax+b)=\frac{\exp\{-b^2\}/\sqrt{\pi}-b\,\operatorname{erfc}(b)}{a} , \qquad a>0 \tag{3.14}$$

the remaining integral can be performed. In the limit $n\to\infty$ the resulting asymptotic rate reads

$$k=\frac{\sqrt{\epsilon}}{uL}\left\{\left[\frac{u^2}{u^2-1}\right]^{1/2}\frac{e^{-(u^2-1)v^2/u^2}}{\sqrt{\pi}} +v\,\operatorname{erfc}\left[-\left[\frac{u^2-1}{u^2}\right]^{1/2}v\right]\right\} . \tag{3.15}$$

TABLE IV. The theoretical rate k given by (3.15) at different values of the parameters ϵ/L^2 and $v=(L/\sqrt{\epsilon})[u-2]/2$. The number below the theoretical rate is the relative difference in percent $100[k_{\text{num}}-k]/k$ to the numerical rate k_{num} from numerical calculations of the probability densities $W_n(x)$ as described at the end of Sec. II but for the hyperbolic map (3.1). The numerical precision is about 0.1%. The numerical effort becomes very large for small ϵ/L^2 and large negative v. For $v=1$ and -2 the relative differences $100[k_{\text{num}}-k_{\text{asymp}}]/k_{\text{asymp}}$ to the asymptotic theoretical rates k_{asymp} in (3.4) and (3.5) are of the order 4% and 40%, respectively. Theoretically, the relative difference between the numerical and analytical rates are predicted to be of the order $O(k)$ for $u\geq 2$ and $[O(k)+O(2-u)]$ for $u<2$, where the additional term $O(2-u)$ is introduced through the approximation of the denominator in (3.3) by $W_{n-1}(-L/2)L/2$. When one uses the same approximation also for the evaluation of the numerical rate k_{num} one obtains considerably smaller relative differences $100[k_{\text{num}}-k]/k$ to the theoretical rate k in (3.15) as given by the numbers in parentheses. Also for $u\geq 2$ the results are slightly improved in this way. For large negative v the deviations are now mainly governed by exponentially small terms in ϵ similar to the situation in Sec. II. For some parameter values for which the numerical effort remains reasonable, we also determined numerical rates k_{num} from simulations of the Langevin equation (2.1) analogous to those described at the end of Sec. II. These results are again given in the form of relative differences $100[k_{\text{num}}-k]/k$ to the theoretical rates k in (3.15) as third lines in the table.

$v=\frac{L}{\sqrt{\epsilon}}\frac{u-2}{2}$	-2	-1	0	1
$\frac{\epsilon}{L^2}=10^{-2}$	5.410×10^{-4}	5.569×10^{-3}	3.257×10^{-2}	9.449×10^{-2}
	82 (12)	36 (4.7)	10 (1.6)	1.3 (0.3)
	78.5	35		
$\frac{\epsilon}{L^2}=10^{-3}$	7.871×10^{-5}	1.479×10^{-3}	1.030×10^{-2}	3.194×10^{-2}
	28 (2.1)	15 (1.2)	4.9 (0.5)	0.7 (0.1)
		15.3	4.2	
$\frac{\epsilon}{L^2}=10^{-4}$	2.068×10^{-5}	4.450×10^{-4}	3.257×10^{-3}	1.033×10^{-2}
	11 (0.7)	5.9 (0.3)	2.0 (0.1)	0.3 (<0.1)
		6.1	1.9	
$\frac{\epsilon}{L^2}=10^{-5}$	6.194×10^{-6}	1.386×10^{-4}	1.030×10^{-3}	3.289×10^{-3}
	4.2 (0.2)	2.3 (<0.1)	0.8 (<0.1)	0.1 (<0.1)
				0.7
$\frac{\epsilon}{L^2}=10^{-6}$	1.926×10^{-6}	4.363×10^{-5}	3.257×10^{-4}	1.042×10^{-3}
	1.6 (<0.1)	0.7 (<0.1)	0.3 (<0.1)	<0.1 (<0.1)

This rate expression is compared in Table IV with the asymptotic rates both from numerical integration of the master equation and similar simulations of the Langevin equation, such as those explained at the end of Sec. II. The different numerical methods yield basically identical results which can be viewed as the exact ones. For sufficiently small noise strengths ϵ, the theoretical rate (3.15) agrees very well with the numerical results. For large ϵ, the deviations of the theoretical rates from the exact values have two origins, namely, the deviations of the approximated density (3.11) from the exact time-dependent solution of the master equation (2.5) for the map (3.1) and the approximate treatment of the integral in the denominator of the rate (3.3). In order to estimate the influence of the latter approximation, we implemented the same approximation in the rate calculation based on the numerical integration of the master equation. The resulting rates deviate considerably less from the theoretical rate; see Table IV. Hence a major part of the errors can be avoided by a more careful evaluation of the denominator of the rate. Closer inspection shows that the approximate solution of the master equation leads to a relative error of the order of the rate itself.

For $u>2$ both conditions $u-2\ll 1$ and $L\gg\epsilon$ are necessary for a sufficient separation of times scales, whereas for $u<2$, the condition $u-2\ll 1$ is of technical nature in order to simplify the determination of the rate. In the excluded parameter range rates may be obtained by means of the methods developed in Ref. [10]. The restricted range of parameters considered here still allows arbitrary values of v, in particular, $|v|$ may be considerably larger than unity. For $v\gg 1$ the first term on the rhs of (3.15) can be neglected and the complementary error function approaches $\mathrm{erfc}(-\infty)=2$, yielding the correct limiting behavior (3.4). For $v\ll -1$ one can make use of the expansion (2.19) in the second term on the rhs of (3.15) leading to the correct limiting behavior (3.5).

For $u=2$ one has $v=0$ and (3.15) takes the simple form

$$k=\frac{\sqrt{\epsilon}}{\sqrt{3\pi}L}\ . \tag{3.16}$$

This case has also been investigated in [23] with the result [see Eq. (4.6) in [23] with $\alpha=0$, $\beta=\frac{1}{2}$, and $2\epsilon/L$ instead of ϵ]

$$k=\frac{\sqrt{\epsilon}}{\sqrt{\pi}L}\,\frac{5-\sqrt{5}}{4}\ . \tag{3.17}$$

This differs by about 20% from (3.16) and also from the numerical simulations in Table IV. In the numerical simulations shown in Fig. 8 of Ref. [23] such deviations can hardly be distinguished. The case $v\ll -1$ has also been considered in Ref. [23] resulting in an exponentially leading part of the form $\exp\{-v^2\}$ [see Eq. (4.5a) in Ref. [23]] in contrast to our analytic result $\exp\{-[(u^2-1)/u^2]v^2\}$, see (3.5), and also our numerical simulations. As already stated below (3.4), the reason for these deviations is that in Ref. [23] only direct exits that pass near $x=-L/2$ are taken into account while those crossing the unstable points as well as possible recrossings are neglected.

If in Eq. (3.15) u is approximated by 2, but not in v, the rate assumes a scaling form as a function of the two small parameters $u-2$ and $\sqrt{\epsilon}/L$:

$$k=\sqrt{\epsilon}/L\,g([u-2]L/\sqrt{\epsilon})\ . \tag{3.18}$$

For fixed L this agrees with the general scaling law $k=\epsilon^{\alpha}F([u-2]\epsilon^{-\beta})$ found in [26]. The dependence of the rate on the ratio of $L/\sqrt{\epsilon}$ is a consequence of the invariance of the Langevin equation (2.1) under the parameter rescaling $L\mapsto cL,\epsilon\mapsto c^2\epsilon$, with an arbitrary $c>0$.

The same analysis can be generalized to maps $f(x)$ consisting of $M\geq 2$ linear pieces with unstable fixed points at $x=0$ and $-L$. On the intervals $I_i:=[x_{i-1},x_i)$, $i=1,2,\ldots,M$, $x_0=-\infty$, $-L<x_1<x_2<\cdots<x_{M-1}<0$, $x_M=+\infty$ the map $f(x)$ may have different constant slopes $f'(x)=u_i$ and extremal values $\Delta_i^+:=\max_{x\in I_i}f(x)$ and $\Delta_i^-:=-L-\min_{x\in I_i}f(x)$. As for $|u-2|$ in the previous case with $M=2$, the moduli $|\Delta_i^{\pm}|$ are assumed to be small. For the asymptotic escape rates k_+ and k_- towards $\pm\infty$, respectively, one finds that

$$k_+=\frac{1}{2L}\sum_{i=1}^{M-1}\frac{1}{|u_i|}\left\{\left[\frac{u_M^2\epsilon}{(u_M^2-1)\pi}\right]^{1/2}\times\exp\left[-\frac{u_M^2-1}{u_M^2\epsilon}(\Delta_i^+)^2\right]+\Delta_i^+\,\mathrm{erfc}\left[-\left[\frac{u_M^2-1}{u_M^2\epsilon}\right]^{1/2}\Delta_i^+\right]\right\}, \tag{3.19}$$

$$k_-=\frac{1}{2L}\sum_{i=2}^{M}\frac{1}{|u_i|}\left\{\left[\frac{u_1^2\epsilon}{(u_1^2-1)\pi}\right]^{1/2}\times\exp\left[-\frac{u_1^2-1}{u_1^2\epsilon}(\Delta_i^-)^2\right]+\Delta_i^-\,\mathrm{erfc}\left[-\left[\frac{u_1^2-1}{u_1^2\epsilon}\right]^{1/2}\Delta_i^-\right]\right\}. \tag{3.20}$$

The full escape rate k is given by the sum $k=k_++k_-$.

As an example we consider a map $f(x)$ with $M=5$ linear pieces of constant slope $u_i=u$ close to 5 and the same value for all quantities Δ_i^+ and Δ_i^- [see Fig. 2, but with $f(x)=ux$ for $x\geq 0$]. Then Eqs. (3.19) and (3.20) simplify to read

$$k_+=k_-=\frac{2}{Lu}\left\{\left[\frac{u^2\epsilon}{(u^2-1)\pi}\right]^{1/2}\exp\left[-\frac{u^2-1}{u^2\epsilon}\Delta^2\right]+\Delta\,\mathrm{erfc}\left[-\left[\frac{u^2-1}{u^2\epsilon}\right]^{1/2}\Delta\right]\right\}, \tag{3.21}$$

where $\Delta:=L[u-5]/8$. This formula is compared with numerical results in Table V.

TABLE V. The theoretical rate k_+ given by (3.21) for a map with five linear pieces at different values of the parameters ϵ/L^2 and $\Delta L/\sqrt{\epsilon}$. The full theoretical escape rate is given by $k=2k_+$. The number below is the relative difference in percent $100[k_{\text{num}}-k]/k$ to the numerical rate k_{num} from iterations of the master equation. For comparable values of the parameters the rates $k=2k_+$ are rather close to those of Table IV, whereas the relative differences of the theoretical and numerical rates are reduced by about a factor of 2.

$\Delta\frac{L}{\sqrt{\epsilon}}$	-1	0	1
$\frac{\epsilon}{L^2}=10^{-2}$	2.694×10^{-3}	2.303×10^{-2}	7.081×10^{-2}
	22	5.9	0.6
$\frac{\epsilon}{L^2}=10^{-3}$	7.345×10^{-4}	7.283×10^{-3}	2.473×10^{-2}
	8.8	2.8	0.3
$\frac{\epsilon}{L^2}=10^{-4}$	2.227×10^{-4}	2.303×10^{-3}	8.089×10^{-3}
	3.8	1.1	0.1

Note that for $\Delta>0$ the ratio of the rates at noise ϵ and at zero noise, $\kappa=k_+(\epsilon)/k_+(0)$, only depends on the system parameters through the combination $\sqrt{u^2\epsilon/(u^2-1)}/\Delta$. Moreover it increases monotonically with increasing noise and hence does not exhibit a stabilization of transient chaos by noise [21]. It can be shown that this atypical behavior is caused the piecewise linearity of the map $f(x)$ in the neighborhood of the extremal points [29].

IV. DECAY OF A POINT ATTRACTOR ACROSS A STRANGE INVARIANT SET

In this section we investigate the Langevin equation (2.1) for a piecewise linear map $f(x)$ which is a combination of the maps considered in Secs. II and III: On $\mathbb{R}_+$ $f(x)$ has a point attractor at $x_s>0$ with an unstable fixed point at $x=0$. On $\mathbb{R}_-$ $f(x)$ is a hyperbolic map near the crisis at fully developed chaos. It has a strange invariant set located between the unstable fixed points at $x=0$ and $-L$. Thus, beyond the crisis the strange repeller on $I:=[-L,0]$ represents the basin boundary of the point attractor x_s, whereas at and below the crisis there are two distinct attractors separated by an unstable fixed point at the origin. A particular example is shown in Fig. 2.

Now we ask about the probability $P(n)$ of a trajectory starting at the stable fixed point x_s to pass a threshold x_{th} after n steps for the first time. The threshold x_{th} lies sufficiently far below $-L$ such that a recrossing of $-L$ can safely be neglected. Numerical results for $P(n)$ obtained from simulations of the Langevin equation are shown in Fig. 3.

In order to understand the behavior of $P(n)$ we discuss a typical realization of the Langevin equation (2.1) for weak noise: A trajectory starting near x_s will stay in $\mathbb{R}_+$ for a long time until it eventually passes the unstable fixed point at the origin. Though the trajectory will typically stay for quite a number of times steps within a small

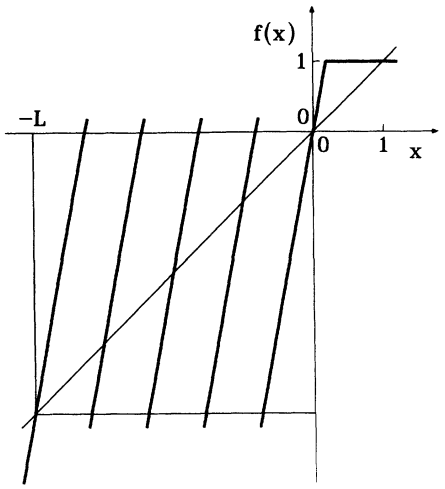

FIG. 2. Typical example of a piecewise linear map $f(x)$ considered in Sec. IV. At $x_s=1$ there is a superstable fixed point, $f(x)\equiv1$ for $x\geq1/u$, and below $x=1/u$ there are five linear pieces of constant slope $u\simeq5$ with unstable fixed points at $x=0$ and $-L$ and discontinuities at $y_i:=-L[2i(u-1)-(u-5)]/[8u]$, $i=1,2,3,4$, defined by $f(x)=ux$ for $y_1\leq x<1/u$, $f(x)=u[x-(y_i+y_{i+1})/2]-L/2$ for $y_{i+1}\leq x<y_i$, $i=1,2,3$, and $f(x)=u[x+L]-L$ for $x<y_4$. The particular parameter values we have chosen in this plot are $L=4$ and $u=5.4$.

vicinity of this fixed point and may recross $x=0$ several times, it will leave the neighborhood of $x=0$ after a much shorter time than the one spent at the attractor and will either return to the attractor or go to the invariant set within the interval $[-L,0]$. There it stays for another long period of time. Eventually, the trajectory will again visit a boundary region for a comparatively short time, followed by the next long sojourn in one of the domains $[0,\infty]$, $[-L,0]$, or $[-\infty,-L]$. Since on the long time scales of the visits of the intervals $[0,\infty]$, $[-L,0]$, and $[-\infty,-L]$ the trajectory loses its memory on where it exactly entered these intervals, each interval can be considered as one single state. Because of this loss of memory and because of the short sojourn times in the boundary regions of these intervals, the coarse grained three-state process is Markovian. The three states denoted by 1, 2, and 3 correspond to the intervals $[0,\infty]$, $[-L,0]$, and $[-\infty,-L]$, respectively. The transition rate k_{21} from state 1 to state 2 describes the decay of a stable fixed point over an unstable one and hence is given by rate (2.18), i.e., $k_{21}=k$. The rates k_{12} and k_{32} from state 2 to the states 1 and 3 describing the decay of the chaotic repeller are given by k_+ and k_-, see Eqs. (3.19) and (3.20), respectively. By construction, state 3 is a limbo state, i.e., the probability to leave it is zero: $k_{13}=k_{23}=0$. Since the probability to go directly from the interval $[0,\infty]$ to $[-\infty,-L]$ is negligibly small, the transition probability from state 1 to 3 also is zero: $k_{31}=0$.

Since all inverse rates are assumed to be much larger than the unit time step we make a continuous-time approximation of the master equations, reading

$$\frac{dP_1(n)}{dn} = -kP_1(n) + k_+ P_2(n) , \tag{4.1}$$

$$\frac{dP_2(n)}{dn} = kP_1(n) - (k_+ + k_-)P_2(n) , \tag{4.2}$$

$$\frac{dP_3(n)}{dn} = k_- P_2(n) , \tag{4.3}$$

where $P_i(n)$ denotes the probability to stay in state i at time n. Since all realizations start at $x_0 = x_s$, the initial conditions are $P_1(0)=1$, $P_2(0)=0$, and $P_3(0)=0$.

The primary quantity of interest is the probability $P(n)=dP_3(n)/dn$ that a realization arrives at the limbo state at time n. A simple calculation yields

$$P(n) = (\lambda_-^{-1} - \lambda_+^{-1})(e^{-\lambda_- n} - e^{-\lambda_+ n}) , \tag{4.4}$$

where

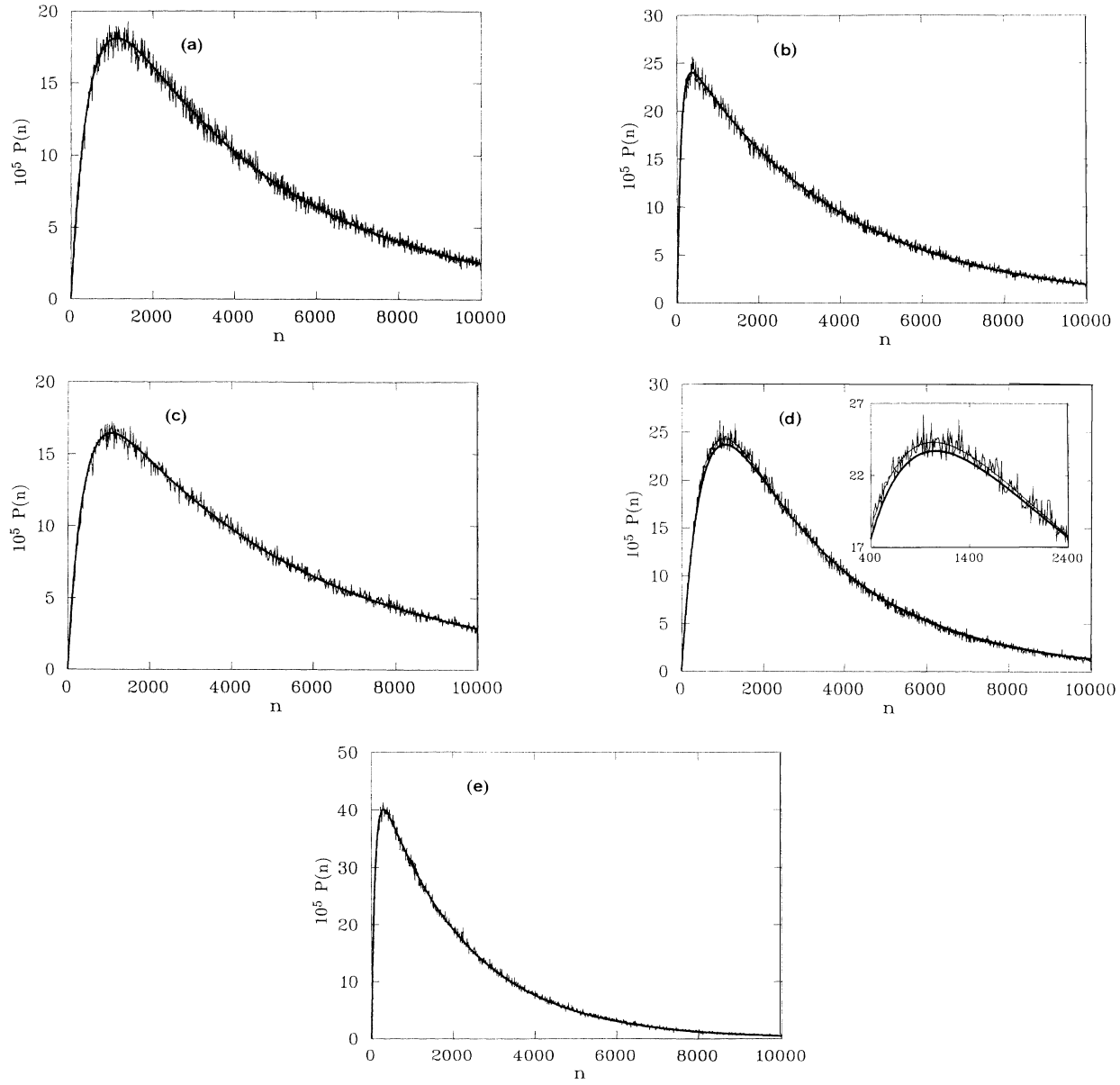

FIG. 3. The probability $P(n)$ to leave the interval $[x_{\rm th}, \infty]$ for the first time after n time steps from $N = 5 \times 10^5$ numerical realizations of the Langevin equation (2.1) with initial condition $x_0 = x_s$. The map $f(x)$ is given by the example of Fig. 2. The threshold $x_{\rm th}$ is chosen at $x_{\rm th} = -L - 1$. The bold curves represent the theoretical predictions (3.21) and (4.4)–(4.6) of the Markovian three-state model. The parameter values are (a) $u = 5$, $\epsilon = 0.18$, and $L = 100$; (b) $u = 5$, $\epsilon = 0.18$, and $L = 20$; (c) $u = 5$, $\epsilon = 0.24$, and $L = 500$; (d) $u = 4.8$, $\epsilon = 0.2$, and $L = 17$; and (e) $u = 5.05$, $\epsilon = 0.2$, and $L = 71$. Thus for (a), (d), and (e) $k \simeq k_+ \simeq 10^{-3}$; (b) $10^{-2} \simeq k_+ \ll k \simeq 10^{-3}$; and (c) $10^{-2} \simeq k \ll k_+ \simeq 10^{-3}$, according to Eqs. (3.21) and (4.6). The very small values of the numerical $P(n)$ for the first few n are an initial effect similar to the behavior shown in Fig. 1. The differences of the numerical and theoretical results are of the same order as the respective errors of the rates k and k_+ at the same parameter values. In (d), the thin curve represents $P(n)$ given by (4.4) and (4.5) but with fitted rates k and k_+, thus indicating the excellent agreement of the simulations with the Markovian three-state model. In the other cases (a)–(c) and (e), such a fitted model cannot be distinguished from the theoretical results.

$$\lambda_{\pm}=\frac{k+k_{+}+k_{-}}{2}\pm\left[\left[\frac{k+k_{+}+k_{-}}{2}\right]^{2}-k_{+}k_{-}\right]^{1/2}. \tag{4.5}$$

For a comparison of this model with numerical simulations of the Langevin equation (2.1) one has to take into account that these simulations become extremely expensive for small noise strengths ϵ. Accordingly, the map $f(x)$ has to be chosen such that for reasonable noise strengths ϵ the agreement between numerical and analytical results is already good for the single rates k, k_{+}, and k_{-}. The comparison of theoretical and numerical results in Tables II–V suggests that the map $f(x)$ as shown in Fig. 2 should be a suitable example for our purposes. This map consists of five linear pieces with constant slope $u\simeq 5$ leading to a strange invariant set on $[-L,0]$ close to a crisis and an additional linear piece of vanishing slope yielding a superstable point attractor at $x_s=1$. Thus the free parameters are L, ϵ, and u with the restrictions $\sqrt{\epsilon}\ll L$, $\sqrt{\epsilon}\ll x_s=1$, and $|u-5|\ll 1$. The rate k following from (2.18) reads

$$k=\tfrac{1}{2}\,\mathrm{erfc}\left[\left[\frac{u^2-1}{\epsilon u^2}\right]^{1/2}\right], \tag{4.6}$$

whereas k_{+} and k_{-} are given by (3.21).

The comparison of $P(n)$ given by (4.4)–(4.6) and by the numerical simulations is shown in Fig. 3. We find excellent agreement and conclude that the description of the decay as the difference of two exponential functions (4.4) is essentially correct. This becomes approximately equal to a simple exponential decay only for very large times $n\gg 1/\lambda_{-}$, which in many situations may be beyond the interesting regime. Possible deviations as those in Fig. 3(d) may be traced back to errors in the theoretical rates. Using the functional form (4.4) for $P(n)$ with $\lambda_{\pm}$ as fit parameters much better agreement with the numerical results is obtained; see Fig. 3(d). The fitted values for λ_{+} and λ_{-} agree with those following from Eq. (4.5) with k, k_{+}, and k_{-} determined by numerical simulations of the decay rates of the respective individual states. Hence the three-state Markovian model provides a correct description of the decay of a state with a fractal basin boundary.

Finally we consider a slightly different situation with $\Delta>0$ where a reflecting boundary at $x=-L$ is imposed. In this way an escape to $-\infty$ is prevented. In the master equation this situation is described by putting $k_{-}=0$. After a sufficiently long time the system reaches an equilibrium in which the ratio of probabilities of the states 2 and 1 coincides with that of the rates k and k_{+}. Using the explicit expressions (3.21) and (4.6) one obtains

$$\frac{P_2}{P_1}=\frac{Lu}{4\Delta}\,\frac{\mathrm{erfc}(\sqrt{\hat{U}/\epsilon})}{\left[\frac{\epsilon}{\hat{U}\Delta^2\pi}\right]^{1/2}e^{-\hat{U}\Delta^2/\epsilon}+\mathrm{erfc}(-\sqrt{\hat{U}\Delta^2/\epsilon})}, \tag{4.7}$$

where $\hat{U}:=[u^2-1]/u^2$. The ratio (4.7) vanishes for $\epsilon=0$. For increasing noise it grows and even for small values of ϵ it may exceed unity if L is sufficiently large. Although the transient chaos in state 2 is not directly enhanced by noise (see the discussion at the end of Sec. III), the destablization of the point attractor in state 1 increases the population of state 2 and leads to so-called noise induced chaos [16,30].

V. SUMMARY AND DISCUSSION

We investigated the decay of metastable states in one-dimensional systems in discrete time caused by the action of weak Gaussian white noise. We compared the results of an analytical theory with the findings of both simulations of a Langevin equation and a numerical integration of the corresponding master equation. Since closed analytical expressions are not available for general noisy nonlinear maps [10], the theory and numerical work were carried out for piecewise linear maps with additive noise. We expect, however, that many qualitative aspects still hold for more general maps. For example, the rate of decay of a deterministically stable point attractor over an unstable fixed point will have the form of an Arrhenius law. The activation energy can be identified with the difference of a generalized potential taken at the stable and the unstable fixed points. The generalized potential follows directly from the invariant density of the noisy map [3]. The leading part of the preexponential factor is determined by local properties of the linearized noisy maps in the vicinities of the stable and unstable fixed points. Additionally, the prefactor contains a globally determined parameter which defines the location of singularities of the generalized potential [10]. Higher order corrections of the prefactor will depend on further details of the map. For decay rates of strange attractors and strange repellers the situation is more complicated. There, not only the linearized maps near the unstable exit points matter but also the analytical behavior of the map at its critical points [29]. However, many other general aspects are expected to be correctly described by the piecewise linear maps such as, e.g., noise induced chaos. The validity of a Markovian three-state model for the decay of a simple attractor with a strange basin boundary certainly holds generally. Multiplicative noise can be dealt with by the same methods and leads to qualitatively similar results as long as the noise couples to the system by a bounded nowhere vanishing function of the state coordinate x.

The theoretical determination of the decay rate is based on the idea of the reactive flux method [11]: The population of the basin of the initial attractor decays with a time-dependent rate that, on a short time scale compared to the inverse rate, approaches a plateau value. From an approximate solution of the master equation for a map with a stable and an unstable fixed point the corresponding time-dependent rate has been derived which rapidly approaches a constant value. This asymptotic rate contains algebraic finite noise corrections to a previously obtained weak-noise result [10,12]. The extension of this method to more general cases such as, for exam-

ple, smooth maps and colored noise, will be presented elsewhere.

By means of a similar method the decay of a strange attractor and a strange repeller has been investigated. In contrast to previous results [23–27], the present theory fully accounts for all typical escape processes and for recrossings of trajectories that already had left an interval containing the invariant set. The different limiting cases below and above the crisis are correctly described: For a map with a chaotic attractor disturbed by weak noise one obtains an Arrhenius-type rate similar to that of a point attractor; the decay rate of a strange repeller approaches its deterministic value when the noise vanishes. In the general case, near the crisis the rate obeys the scaling law derived in [26].

By means of numerical simulations we finally studied the decay law of a single attractor with a basin boundary consisting in a strange repeller. The numerical results agree excellently with a Markovian model with three states; one corresponds to the interior of the basin of the point attractor, the second one to an interval containing the repeller, and the third one is an absorbing state. The decay is then determined by two exponents that follow from the individual decay rates of the point attractor and the strange repeller. The generalization to the case of deterministic diffusion above a crisis [25,29] disturbed by external noise is straightforward.

ACKNOWLEDGMENTS

We thank W. Breymann and C. Van den Broeck for valuable discussions. P.R. is indebted to the theoretical physics group at the Limburgs Universitair Centrum for the kind hospitality during the completion of this work. Financial support by the Swiss National Science Foundation, the Freiwillige Akademische Gesellschaft, Basel, the Program on Inter-University Attraction Poles of the Belgian Government, and the Alexander von Humboldt Foundation is gratefully acknowledged.

[1] H. A. Kramers, Physica **7**, 284 (1940).
[2] P. Hänggi, P. Talkner, and M. Borkovec, Rev. Mod. Phys. **62**, 251 (1990).
[3] P. Reimann and P. Talkner, Phys. Rev. A **44**, 6348 (1991).
[4] Yu. Kifer, *Random Perturbations of Dynamical Systems* (Birkhäuser, Boston, 1988).
[5] P. Talkner, P. Hänggi, E. Freidkin, and D. Trautmann, J. Stat. Phys. **48**, 231 (1987).
[6] P. Talkner and P. Hänggi, in *Noise in Nonlinear Dynamical Systems,* edited by F. Moss and P. V. E. McClintock (Cambridge University Press, Cambridge, 1989), Vol. 2.
[7] A. Hamm and R. Graham, J. Stat. Phys. **66**, 689 (1992).
[8] H. Risken, *The Fokker-Planck Equation* (Springer, Berlin, 1984).
[9] For a review see R. Graham, in *Noise in Nonlinear Dynamical Systems* (Ref. [6]), Vol. 1.
[10] P. Reimann and P. Talkner, in *New Trends in Kramers' Reaction Rate Theory,* edited by P. Talkner and P. Hänggi (Kluwer, Dordrecht, in press).
[11] D. J. Chandler, J. Chem. Phys. **68**, 2959 (1978).
[12] P. Reimann and P. Talkner (unpublished).
[13] For a review see T. Tél, in *Directions in Chaos,* edited by Hao Bai-lin (World Scientific, Singapore, 1990), Vol. 3.
[14] B. B. Mandelbrot, *The Fractal Geometry of Nature* (Freeman, New York, 1977); S. W. McDonald, C. Grebogi, E. Ott, and J. A. Yorke, Physica D **17**, 125 (1985).
[15] *Noise in Nonlinear Dynamical Systems,* edited by F. Moss and P. V. E. McClintock (Cambridge Univeristy Press, Cambridge, 1989), Vols. 1–3.
[16] R. L. Kautz, J. Appl. Phys. **58**, 424 (1985); M. Iansiti, Qing Hu, R. M. Westervelt, and M. Tinkham, Phys. Rev. Lett. **55**, 746 (1985).
[17] Junli Liu and S. K. Scott, J. Chem. Phys. **94**, 4416 (1991).
[18] E. G. Gwinn and R. M. Westervelt, Phys. Rev. Lett. **54**, 1613 (1985).
[19] P. E. Phillipson and A. J. Armstrong, Phys. Lett. A **146**, 401 (1990).
[20] P. Grassberger, J. Phys. A **22**, 3283 (1989).
[21] M. Franaszek, Phys. Rev. A **44**, 4065 (1991).
[22] C. Grebogi, E. Ott, and J. A. Yorke, Phys. Rev. Lett. **48**, 1507 (1982).
[23] S. Takesue and K. Kaneko, Prog. Theor. Phys. **71**, 35 (1984).
[24] P. D. Beale, Phys. Rev. A **40**, 3998 (1989).
[25] T. Geisel and J. Nierwetberg, Phys. Rev. Lett. **48**, 7 (1982).
[26] F. T. Arecchi, R. Badii, and A. Politi, Phys. Lett. **103A**, 3 (1984).
[27] J. C. Sommerer, E. Ott, and C. Grebogi, Phys. Rev. A **43**, 1754 (1991).
[28] R. García-Pelayo and W. C. Schieve, J. Math. Phys. **33**, 570 (1992).
[29] P. Reimann (unpublished).
[30] F. T. Arecchi, R. Baddi, and A. Politi, Phys. Rev. A **29**, 1006 (1984); H. Herzel, W. Ebeling, and Th. Schulmeister, Z. Naturforsch. A **42**, 136 (1987); V. S. Anishchenko and H. Herzel, Z. Angew. Math. Mech. **68**, 317 (1988).